Check for updates

OPEN

Research and application of rock fracturing pressure prediction method for deep oil reservoirs

Yanlin Zhang[1,4], Yang Tian[2✉], Lina Sun[3], Zhufeiye Yuan[2✉] & Yi Wang[4]

The combination of extreme formation pressure, significant burial depth, and dense lithology in deep and ultra-deep reservoirs results in abnormal fracturing pressure behavior. This phenomenon elevates operational pressures during fracturing acidizing treatments while amplifying associated engineering risks. Precise prediction of both reservoir fracturing pressure and pump injection pressure has become imperative under current technological constraints to ensure operational safety and successful reservoir stimulation. This study establishes a comprehensive fracturing pressure prediction framework through: Developing rock fracturing pressure models for open-hole and perforated completions based on near-wellbore stress distribution characteristics. Investigating fracture initiation mechanisms and corresponding computational models for perforation-altered stress fields. Deriving damage-adapted calculation models that account for stress variations in both completion types under formation impairment conditions. Numerical simulations demonstrate critical findings revealed that perforated completions reduce reservoir fracturing pressure by 10–15% compared to open-hole configurations, proving effective for pressure management. Formation damage induces stress redistribution, increasing fracturing pressure by 8–12%—a crucial factor for treatment design optimization. Maximum pressure reduction (18–22%) occurs when perforation orientation aligns within ± 40° of the maximum horizontal stress direction, beyond which fracture deviation triggers abrupt pressure escalation. Perforation density shows linear correlation with pressure reduction (3–5% decrease per 2 shots/m increase), while perforation dimensions exhibit limited impact (< 1% variation). The developed multi-completion prediction methodology provides dual engineering benefits: It enhances operational safety for hydraulic fracturing in deep reservoirs through reliable pressure forecasting, while serving as a strategic optimization tool for completion design—particularly in maximizing hydrocarbon recovery from challenging deep formations. This approach establishes a critical technical foundation for economically viable development of deep petroleum resources.

Keywords Deep oil reservoirs, Completion methods, Stress distribution, Fracturing pressure, Reservoir damage

Recent advancements in China's oil and gas exploration technologies have enabled significant breakthroughs in developing deep, tight, and low-permeability reservoirs. Notably, over 60% of these reservoirs exhibit abnormally high fracturing pressures (typically exceeding 80 MPa), presenting unique engineering challenges[1–5]. While hydraulic fracturing and acid stimulation remain indispensable for reservoir evaluation and production enhancement, practitioners continue to face two persistent technical bottlenecks: (1) formation breakdown failures during fracturing operations, and (2) fluid injection difficulties in acidizing treatments. These operational constraints significantly impede effective reservoir stimulation and production optimization in ultra-deep (> 6500 m) unconventional plays[6–10].

The genesis of abnormal fracturing pressures in subsurface formations stems from a complex interplay of geological and engineering factors. Primary contributors include excessive horizontal stress anisotropy (> 1.5 stress ratio), pronounced lithological heterogeneity (variations exceeding 30% in Young's modulus), elevated clay content (> 35% smectite-rich formations), and suboptimal perforation phasing alignment (> 15° deviation from principal stress orientation)[11,12]. At the core of hydraulic fracturing research lies two

[1]College of Resources and Environment, Yangtze University, Wuhan 430100, Hubei, China. [2]School of Geosciences, Yangtze University, Wuhan 430100, Hubei, China. [3]Cooperative Innovation Center of Unconventional Oil and Gas (Ministry of Education and Hubei Province), Yangtze University, Wuhan, Hubei Geological Survey, Wuhan 430100, Hubei, China. [4]Hubei Geological Survey, Wuhan 430034, Hubei, China. ✉email: ty@yangtzeu.edu.cn; 2022710399@yangtzeu.edu.cn

fundamental questions: (1) precise fracture initiation timing determination, and (2) comprehensive propagation mechanism elucidation[13–15]. Numerous scholars have committed themselves to this field and have proposed criteria for identifying fracture patterns during the hydraulic fracturing process based on various mechanical theories[14,16,17]. These criteria can be broadly categorized into two types: one pertaining to elastic mechanics models and the other related to fracture mechanics models[18]. Hubbert's seminal work established the classical tensile failure criterion under idealized conditions of homogeneous, isotropic, impermeable elastic media[19,20]. This approach focuses on borehole wall tangential stresses (σ_θ) while neglecting vertical (σ_v) and radial (σ_r) stress components' synergistic effects[21,22]. As a natural medium, rock mass typically contains inherent fractures; particularly in scenarios where fracture development is pronounced or artificial fractures are present, it becomes essential to analyze rock mass failure induced by hydraulic fracturing through fracture mechanics theory[23,24]. Essential for naturally fractured reservoirs, this paradigm addresses hydraulic fracture interaction with pre-existing discontinuities. Vallejo's dam studies revealed that fracture propagation predominantly follows mixed-mode (I-II) mechanisms rather than pure Mode I extension[23,24]. Crucially, his work demonstrates that fracture advancement can occur through shear-dominated (Mode II) mechanisms without requiring normal tensile stresses, particularly in scenarios with significant pre-existing fracture networks[25].

Experimental research serves as an effective and intuitive method for investigating the hydraulic fracturing mechanisms of rocks. Since the inaugural successful hydraulic fracturing test was conducted in the United States, numerous researchers have engaged in related experimental studies[26,27]. Nobari et al. examined the stress conditions necessary for hydraulic fracturing using a cylindrical specimen with an outer diameter of 3.56 cm, an inner diameter of 0.64 cm, and a height of 8.90 cm[28]. Mori et al. performed hydraulic fracturing experiments on thick-walled cylindrical specimens composed of viscous soil, featuring outer diameters of 5.00 cm, 7.50 cm, and 15.00 cm; inner diameters of 0.40 cm and 0.80 cm; and heights ranging from 1 to 2 times the outer diameter. The findings revealed that the mechanical mechanism underlying hydraulic fracturing is predominantly shear failure rather than tensile failure. Furthermore, provided that the water pressure injection rate is sufficiently high, factors such as liquid viscosity, specimen size, and local fractures near the borehole can be considered negligible regarding their influence on hydraulic fracturing pressure[29].

Cheng et al. conducted field experiments that provided a comprehensive analysis of hydraulic fracturing pressure in rock masses. They asserted that the fracture surface is invariably perpendicular to the direction of the minor principal stress, regardless of whether the liquid can infiltrate the rock mass[30]. In various geological formations, the minor principal stress within surface rock strata may manifest as either horizontal or vertical. Fjaer conducted hydraulic fracturing experiments on rocks via drilling techniques. He asserted that in an impermeable rock mass where the direction of the minimum principal stress is orthogonal to the borehole axis, the pressure required to induce hydraulic fracturing is equivalent to the sum of the rock's tensile strength and twice the minor principal stress[19]. Bjerrum et al. performed hydraulic fracturing tests on a natural clay core wall within a reservoir embankment. The experimental results indicated that when water pressure exceeded 0.40 to 0.50 times the effective self-weight of the overlying soil, there was a sudden increase in permeability, resulting in hydraulic fracturing[31]. A multitude of researchers have focused on numerical simulation studies related to hydraulic fracturing, developing various two-dimensional, pseudo-three-dimensional, or fully three-dimensional numerical tools for this purpose[32–34]. Presently, numerous methods exist for analyzing rock fracture behavior; from a technical standpoint regarding fracture treatment, these can be categorized into continuous deformation numerical methods and discontinuous deformation numerical methods.

Previous research has yielded a relatively comprehensive understanding of the qualitative characterization of rock fracture and the prediction of fracturing pressure. However, the influence mechanisms of various completion techniques on the fracturing pressure of reservoir rocks remain inadequately defined. Furthermore, following reservoir damage, alterations in fracturing pressure have occurred, leading to significant variability and subjectivity in selecting appropriate technologies for predicting reservoir rock fracturing pressure and optimizing fracturing operation parameters. Therefore, it is imperative to conduct further investigations into predictive methodologies for reservoir fracturing pressure under complex geological conditions and diverse completion strategies to facilitate the efficient development of deep, tight, low-permeability oil and gas reservoirs characterized by exceptionally high fracturing pressures.

By comprehensively integrating pertinent theories such as rock mechanics and elasticity theory, and based on the analysis of in-situ stress surrounding the wellbore, models for rock fracturing pressure in both open-hole and perforated wells were developed. Following the in-situ stress analysis of perforated wells, fracture initiation modes and corresponding fracturing pressure calculation models were thoroughly examined. Furthermore, a detailed investigation was conducted into the in-situ stress characteristics of open-hole and perforated wells post-reservoir damage, resulting in the formulation of formation fracturing pressure calculation models applicable to both completion methods under damaged conditions. Regarding the fracturing pressure models associated with open-hole and perforated completions, calculations for individual well fractures under varying completion scenarios were executed to validate the reliability of the formation fracturing pressure prediction model, which will facilitate advancements in optimizing techniques aimed at reducing formation fracturing pressures.

Prediction model of reservoir fracturing pressure
Geological characteristics of the oil reservoir
The reservoir in the study area is buried at a depth exceeding 6500 m, characterized by weak karstification, leading to relatively dense reservoir development. The porosity primarily ranges from 0.1 to 3.5%, with an average permeability of 0.25×10^{-3} μm^2. Fracture and cavity filling is significant, with fully filled fractures comprising 34.69% and semi-filled fractures accounting for 53.99%. The average density of the reservoir rock is 2.69 g/cm^3, and the overburden pressure is notably high. The primary mineral component of the reservoir rock is calcite, typically exceeding 99%, while secondary minerals such as pyrite, siliceous material, dolomite, and authigenic

quartz collectively constitute less than 1%. The predominant rock types are mud microcrystalline limestone (74.3%), followed by grain limestone (17.4%) and bioclastic limestone (8.3%).

The fracturing pressure of the openhole completed reservoir

The abnormal fracturing pressure is primarily attributed to factors such as deep reservoir burial, high tectonic stress, dense lithology, and reservoir damage. Therefore, it is crucial to establish a quantitative prediction model for the fracturing pressure of the reservoir under various conditions. This model will serve as a basis for reducing stimulation risks and optimizing operations. The wellbore formation disrupts the original stress equilibrium, leading to stress redistribution in the surrounding rock and subsequent stress concentration during fracturing operations. Fractures initiate when the wellbore pressure exceeds the tensile strength of the circumferential stress in the rock. It should be noted that fracture initiation points, fracture azimuths, and fracturing pressures are all dependent on the stress state around the wellbore. To comprehensively study fracture initiation mechanisms, an analysis of the stress state surrounding the wellbore must be conducted first.

Following Biot's poroelastic theory, the effective stress in intact media is defined as $\sigma'_{ij} = \sigma_{ij} - \alpha p \delta_{ij}$, where $\alpha \in [0,1]$ represents the Biot coefficient (Detournay & Cheng, 1993)[35]. However, when evaluating shear failure through Mohr–Coulomb criteria or tensile fracturing, Terzaghi's effective stress $\sigma'_n = \sigma_n - p$ is adopted (Zimmerman, 1991; Segall, 2010)[36,37], consistent with standard geomechanical practice for failure analysis. By considering factors such as initial stresses, fracture fluid forces, and fluid infiltration into the formation, a comprehensive understanding of the stresses acting on the rock around the wellbore can be obtained through the superposition method[38–40].

$$\sigma_r = \frac{\sigma_H + \sigma_h}{2}\left(1 - \frac{r_i^2}{r^2}\right) + \left(\frac{\sigma_H - \sigma_h}{2}\right)\left(1 - 4\frac{r_i^2}{r^2} + 3\frac{r_i^4}{r^4}\right)\cos 2\theta + \frac{r_i^2}{r^2}P_i$$
$$- \alpha P_p + \delta\left[\frac{\alpha(1-2\mu)}{2(1-\mu)}\left(1 - \frac{r_i^2}{r^2}\right) - \phi\right](P_i - P_p) \tag{1}$$

$$\sigma_\theta = \frac{\sigma_H + \sigma_h}{2}\left(1 + \frac{r_i^2}{r^2}\right) - \left(\frac{\sigma_H - \sigma_h}{2}\right)\left(1 + 3\frac{r_i^4}{r^4}\right)\cos 2\theta - \frac{r_i^2}{r^2}P_i$$
$$- \alpha P_p + \delta\left[\frac{\alpha(1-2\mu)}{2(1-\mu)}\left(1 + \frac{r_i^2}{r^2}\right) - \phi\right](P_i - P_p) \tag{2}$$

$$\sigma_z = \sigma_z - 2\mu(\sigma_H - \sigma_h)\frac{r_i^2}{r^2}cos2\theta + \delta\left[\frac{\alpha(1-2\mu)}{1-\mu} - \phi\right](P_i - p_p) - \alpha P_p \tag{3}$$

$$\tau_{r\theta} = \frac{\sigma_H + \sigma_h}{2}\left(1 - 3\frac{r_i^4}{r^4} + 2\frac{r_i^2}{r^2}\right)sin2\theta \tag{4}$$

The circumferential stress at the borehole is as follows.

$$\sigma_\theta = -P_i + \delta\left[\frac{\alpha(1-2\mu)}{1-\mu} - \right](P_i - P_p) + \sigma_H(1 - 2\cos 2\theta) + \sigma_h(1 + 2\cos 2\theta) - \alpha P_p$$
$$= -P_i + (\sigma_H + \sigma_h) - 2(\sigma_H - \sigma_h)\cos 2\theta - \alpha P_p + \delta\left[\frac{\alpha(1-2\mu)}{1-\mu} - \right](P_i - P_p) \tag{5}$$

where, σ_H, σ_h are the maximum and minimum horizontal principal stresses, respectively, MPa. μ is the Poisson's ratio of rocks, Dimensionless. P_p is the pore pressure of formation, MPa. P_i is the pore pressure at point i in the formation, MPa. α is the effective stress coefficient, Dimensionless. r is the radial distance, m. θ is angle of tangential stress, °. ϕ is the rock porosity, Dimensionless. σ_r, σ_θ, σ_z and $\tau_{r\theta}$ is the effective normal stresses in radial, tangential, and vertical directions; and the shear stress, MPa. δ is the coefficient, when the borehole has seepage, $\delta = 1$, and when the borehole has no seepage, $\delta = 0$. P_p is the pore pressure, MPa.

After extensive research and practical application, various fracture initiation criteria have been proposed for fracturing technology. Cai et al. argued that the fracturing pressure predicted by the tensile fracture criterion (maximum tensile stress principle) is more accurate than any other criterion, whether it pertains to small fractures or local stress distribution determined by fracturing test data[41]. Currently, the tensile failure criterion is widely employed in fracturing design to predict fracture initiation based on the rock's tensile fracture characteristics: when subjected to circumferential tensile stress reaching its material tensile strength, new open fault chips will form perpendicular to the direction of the applied tension.

The occurrence of fracture is imminent when the maximum effective tensile stress at the borehole reaches the rock's tensile strength σ_t.

$$\sigma_\theta = -\sigma_t \tag{6}$$

From Eq. (5), as P_i increases, σ_θ decreases, and when P_i increases to a certain extent, σ_θ will become negative, meaning that the axial stress on the rock changes from compression to tension. When the tensile stress is great enough to overcome the rock's tensile strength, the formation will undergo fracture. The fracture occurs at the

specific location where the rock fractures when the stress reaches the critical value σ_θ, and this location is on the direction θ of 0° or 180°, and the value of σ_θ is as follows.

$$\sigma_\theta = 3\sigma_h - \sigma_H - \alpha P_p - P_i + \delta \left[\frac{\alpha(1-2\mu)}{1-\mu} - \phi \right] (P_i - P_p) \tag{7}$$

Substitute the Eq. (7) into the Eq. (6), and the in-well pressure at which the rock undergoes tensile failure can be obtained, also known as the formation fracturing pressure.

$$P_i = \frac{3\sigma_h - \sigma_H - \alpha P_p + \sigma_t - \delta \left[\frac{\alpha(1-2\mu)}{1-\mu} - \phi \right] P_p}{\left\{ 1 - \delta \left[\frac{\alpha(1-2\mu)}{1-\mu} - \phi \right] \right\}} \tag{8}$$

If the filtration of fracturing fluid is not taken into consideration, the fracturing of the formation can be simplified as:

$$P_i = 3\sigma_h - \sigma_H - \alpha P_p + \sigma_t \tag{9}$$

Equation (9) is a commonly used formula for predicting the fracturing pressure.

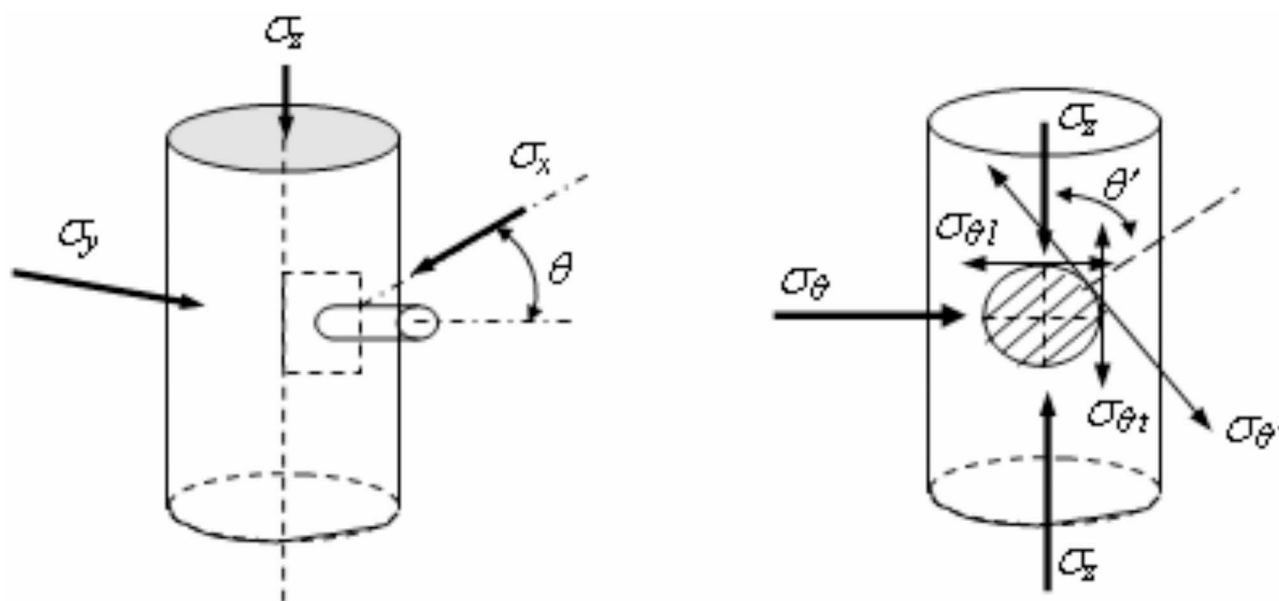### The fracture initiation model for perforated well completion

Compared to naked-eye completion, the calculation of fracturing pressure for perforated completion is more complex, as not only the casing stress on the formation but also the stress on the wellbore and the near-well area caused by the perforation hole has a significant impact.

Stress distribution around perforated well and perforated hole

If the communication between the wellbore formation and the perforation is good, and there is no perforation friction, then the bottom hole pressure is equal to the pressure within the perforation. Before the formation fractures, there is a micro fracture zone at the second interface between the formation and the cement sheath. After perforating, the wellbore can be considered as two orthogonal cylindrical holes of different diameters. The geometric model and stress redistribution model of the perforated wellbore are shown in Fig. 1.

In Fig. 1, σ_z is the axial stress of the wellbore, σ_θ is the tangential stress of the wellbore, $\sigma_\theta{}'$ is the tangential stress of the perforation hole, $\sigma_{\theta l}$ is the concentrated stress that forms longitudinal fractures (vertical fractures), and $\sigma_{\theta t}$ is the concentrated stress that forms transverse fractures (horizontal fractures). According to the principle of stress superposition, the tangential stress at the root of the hole is,

$$\sigma_{\theta'} = (\sigma_H + \sigma_h + \sigma_v) + 2(\sigma_H + \sigma_h - \sigma_v)\cos 2\theta' - 2(\sigma_H - \sigma_h)\left(\cos 2\theta + 2\cos 2\theta \cos 2\theta'\right)$$
$$- 2P_i\left(1 + \cos 2\theta'\right) + 2\delta\left[\frac{\alpha(1-2\mu)}{1-\mu} - \right](P_i - P_o)\left(1 + \cos 2\theta'\right) \tag{10}$$

Fig. 1. Geometric model of perforated wellbore and redistribution of surrounding Earth stress[42].

4

According to the stress distribution model of the open hole wellbore, the stress field distribution around the perforated wellbore can be simplified as

$$
\begin{cases}
\begin{aligned}
\sigma_{\theta'} =\ & (\sigma_H + \sigma_h + \sigma_z) + 2\left(\sigma_H + \sigma_h - \sigma_z\right)\cos 2\theta' \\
& - 2\left(\sigma_H - \sigma_h\right)\left(\cos 2\theta + 2\cos 2\theta \cos 2\theta'\right) \\
& - 2P_i\left(1 + \cos 2\theta'\right) + 2\delta\left[\frac{\alpha\left(1 - 2\mu\right)}{1 - \mu} - \phi\right]\left(P_i - P_o\right)\left(1 + \cos 2\theta'\right)
\end{aligned} \\
\sigma_r = P_i - \delta\phi\left(P_i - P_o\right) \\
\sigma_z = \sigma_v - 2\mu\left(\sigma_H - \sigma_h\right)\cos 2\theta - cP_i + \delta\left[\frac{\alpha\left(1 - 2\mu\right)}{1 - \mu} - \phi\right]\left(P_i - P_o\right)
\end{cases}
\tag{11}
$$

Equation (11) is an approximate analytical expression for the stress distribution around perforated wells, which is widely used nowadays. It can be seen that this expression differs from the expression for open hole wells only in that σ_θ has been changed to σ_θ', emphasizing the stress distribution around the perforation and considering that the perforation is the main site of fracture initiation.

In a small range, stress near the perforation can be obtained using a stress solving method similar to that of an open hole wellbore.

$$
\begin{aligned}
\sigma'_{pr} =\ & \frac{\sigma_\theta + \sigma_z}{2}\left(1 - \frac{r_{perf}^2}{L_{perf}^2}\right) + \frac{\sigma_\theta - \sigma_z}{2}\left(1 - 4\frac{r_{perf}^4}{L_{perf}^4} + \frac{3r_{perf}^4}{L_{perf}^4}\right)\cos 2\theta' + \frac{r_{perf}^2}{L_{perf}^2}P_i - \alpha p_p \\
& + \delta\left[\frac{\alpha\left(1 - 2\mu\right)}{1 - \mu}\left(1 - \frac{r_{perf}^2}{L_{perf}^2}\right) - \right]\left(p_i - p_o\right)
\end{aligned}
\tag{12}
$$

$$
\begin{aligned}
\sigma'_{p\theta} =\ & \frac{\sigma_\theta + \sigma_z}{2}\left(1 + \frac{r_{perf}^2}{L_{perf}^2}\right) - \frac{\sigma_\theta - \sigma_z}{2}\left(1 + \frac{3r_{perf}^4}{L_{perf}^4}\right)\cos 2\theta' - \frac{r_{perf}^2}{L_{perf}^2}P_i \\
& - \alpha p_p + \delta\left[\frac{\alpha\left(1 - 2\mu\right)}{1 - \mu}\left(1 + \frac{r_{perf}^2}{L_{perf}^2}\right) - \right]\left(p_i - p_o\right)
\end{aligned}
\tag{13}
$$

$$
\sigma'_{pz} = \sigma_r - 2\mu\left(\sigma_\theta - \sigma_z\right)\frac{r_{perf}^2}{L_{perf}^2}\cos 2\theta' - cp_w\frac{r_{perf}^2}{L_{perf}^2} + \delta\left[\frac{\alpha\left(1 - 2\mu\right)}{1 - \mu} - \phi\right]\left(p_i - p_o\right) - \alpha p_p
\tag{14}
$$

where, r_{perf} represents the radius of the perforation hole; L_{perf} represents the distance from the perforation hole. Substituting the stresses σ_r, σ_θ, and σ_z around the wellbore obtained from the previous calculations into the stress formula around the borehole yields the stress distribution around the borehole.

The fracturing pressure of perforated well
In practical calculations, considering that the initiation of fractures always starts from the wellbore or perforation hole wall, it is simplified as the stress on the perforation hole wall, which is taken as $r_{perf} = L_{perf}$. Considering that the cement sheath and formation are well consolidated, there will be no seepage of fracturing fluid into the formation. At this time, the pressure on the wellbore is 5% of the fracturing fluid pressure, and due to good consolidation, there will be no filtration of fracturing fluid[43]. Filtration only occurs from the perforation wall, and the pressure of the perforation hole is always equal to the fracturing fluid pressure, that is, $p_{perf} = p_i$. When the cement sheath and the formation are well consolidated, there is no seepage of fracturing fluid through the wellbore to the formation. Therefore, the calculation formula for the geostress around the wellbore becomes that.

$$
\sigma_r = \frac{\sigma_H + \sigma_h}{2}\left(1 - \frac{r_i^2}{r^2}\right) + \left(\frac{\sigma_H - \sigma_h}{2}\right)\left(1 - 4\frac{r_i^2}{r^2} + 3\frac{r_i^4}{r^4}\right)\cos 2\theta + \frac{r_i^2}{r^2}P_i - \alpha P_p
\tag{15}
$$

$$
\sigma_\theta = \frac{\sigma_H + \sigma_h}{2}\left(1 + \frac{r_i^2}{r^2}\right) + \left(\frac{\sigma_H - \sigma_h}{2}\right)\left(1 + 3\frac{r_i^4}{r^4}\right)\cos 2\theta - \frac{r_i^2}{r^2}P_i - \alpha P_p
\tag{16}
$$

$$
\sigma_z = \sigma_z - 2\mu\left(\sigma_H - \sigma_h\right)\frac{r_i^2}{r^2}\cos 2\theta + \delta\left[\frac{\alpha\left(1 - 2\mu\right)}{1 - \mu} - \varphi\right]\left(P_i - p_p\right) - \alpha P_p
\tag{17}
$$

Therefore, the stress on the perforation wall becomes as follows.

$$
\begin{cases}
\sigma'_{pr} = \dfrac{r^2_{perf}}{L^2_{perf}} P_i - \alpha p_p + \delta\varphi\,(p_i - p_o) \\[2mm]
\sigma'_{p\theta} = \left\{
\begin{array}{l}
-P_i + \sigma_H\,(1 - 2cos2\theta) + \sigma_h\,(1 + 2cos2\theta) - \alpha P_p \\[1mm]
+c\dfrac{r^2_i}{r^2}P_i + \sigma_v - 2\mu\,(\sigma_H - \sigma_h)\,cos2\theta - \alpha P_p
\end{array}
\right\} \\[6mm]
\qquad -2\left\{
\begin{array}{l}
-P_i + \sigma_H\,(1 - 2cos2\theta) + \sigma_h\,(1 + 2cos2\theta)_p \\[1mm]
-c\dfrac{r^2_i}{r^2}P_i - \sigma_v + 2\mu\,(\sigma_H - \sigma_h)\,cos2\theta
\end{array}
\right\} cos2\theta' \\[6mm]
\qquad - P_i - \alpha p_p + \delta\left[\dfrac{2\alpha\,(1 - 2\mu)}{1 - \mu} - \varphi\right](p_i - p_o) \\[4mm]
\sigma'_{pz} = -2\mu\left\{
\begin{array}{l}
-P_i + \sigma_H\,(1 - 2cos2\theta) + \sigma_h\,(1 + 2cos2\theta)_p \\[1mm]
-c\dfrac{r^2_i}{r^2}P_i - \sigma_v + 2\mu\,(\sigma_H - \sigma_h)\,cos2\theta
\end{array}
\right\} cos2\theta' \\[6mm]
\qquad + P_i + \delta\varphi\,(P_i - p_p) - \alpha P_p - cp_w \\[2mm]
\qquad + \delta\left[\dfrac{\alpha\,(1 - 2\mu)}{1 - \mu} - \varphi\right](p_i - p_o) - \alpha p_p
\end{cases}
\tag{18}
$$

Therefore, due to the good consolidation between the cement sheath and the formation, fractures cannot occur from the wellbore, but only from the perforation holes. So, take r from r_i to $r_i + d_{perf}$ (hole depth), calculate the σ_z and σ_θ at the selected point in this interval (Eqs. (16) and (17)), substitute into Eq. (18) to solve for $\sigma'_{p\theta}$, and then use this parameter to determine the location of the maximum tensile stress on the hole and the fracturing pressure.

The influence of perforation parameters on the fracturing pressure

Analysis method
The analysis method of the influence of perforation parameters on rock fracture pressure mainly includes the following steps.

a. *Establish a mechanical model*: Based on the principles of rock mechanics and seepage mechanics, and considering the formation conditions, rock properties and perforation operation characteristics comprehensively, a perforation in-situ stress mechanical model including fluid–solid coupling effect and dynamic effect is constructed.
b. *Solve the model using numerical methods*: Use the finite element method or other applicable numerical methods, combined with rock fracture criteria, to solve the model to obtain the in-situ stress distribution state and rock fracture pressure. Analyze the fracture propagation law through the finite element model and evaluate the influence of perforation parameters on rock fracture pressure.
c. *Analyze the influence of perforation parameters*: By changing perforation parameters (such as perforation density, perforation azimuth, perforation hole diameter and perforation depth, etc.), systematically observe and analyze the specific influence of these parameters on rock fracture pressure.

The analysis of the factors influencing the rock fracture pressure by perforation parameters is a comprehensive process, involving the establishment of mechanical models, the solution of numerical methods, and the detailed analysis of the impact of perforation parameters. This process is of great significance for optimizing the design of perforation parameters and improving the effect of fracturing operations.

The perforation parameters mainly include the perforation density, the phase angle and azimuth angle of the perforation eyehole, the diameter of the perforation eyehole, and the penetration depth, etc. The following is an analysis of the influencing factors based on the basic parameters of a typical well.

Result and discussion

① The perforation azimuth

The angle of perforation azimuth is the angle between the perforation axis line and the direction of the maximum horizontal stress, calculated for a perforation density of 16 holes/m using the example of 16 holes/m. By changing the perforation azimuth, the impact of perforation azimuth on fracturing pressure is calculated. Simulation research shows that the stress concentration around the wellbore is a function of the perforation azimuth relative to the maximum horizontal principal stress direction, and the fracturing pressure is a function of the angle between the perforation azimuth and the maximum horizontal principal stress direction. When the perforation hole axis is parallel to the maximum horizontal principal stress direction, the fracturing pressure is lowest; when the perforation hole axis is perpendicular to the maximum horizontal principal stress direction, the fracturing pressure is highest. According to the study, the optimal perforation azimuth for effectively reducing formation fracturing pressure is within the ±40° region of the maximum principal stress
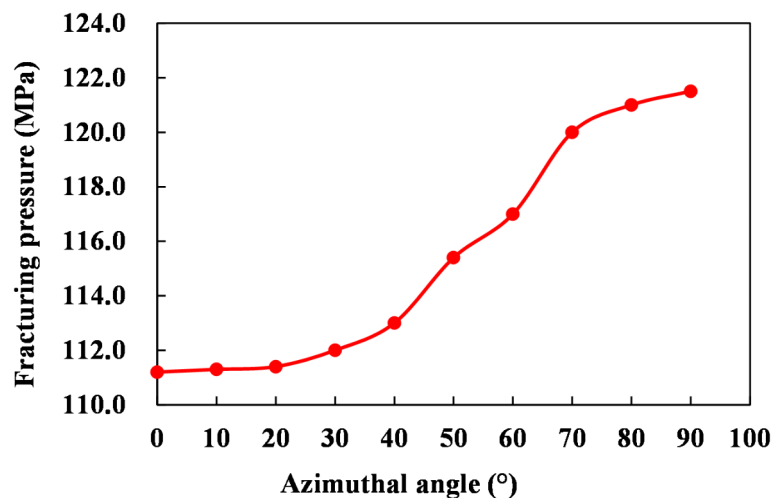
Fig. 2. The relationship between the perforation azimuth of well 1 and its formation fracturing pressure.
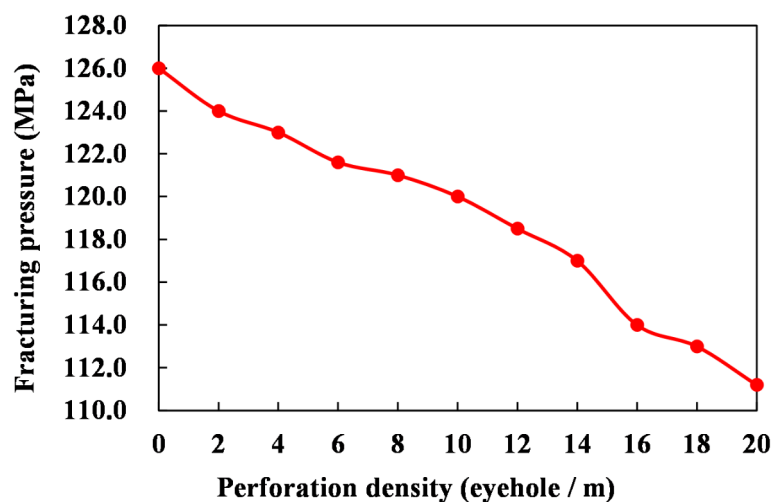

Fig. 3. Relationship between perforation density of well 1 and its fracturing pressure.

direction; beyond this range, it is easy to cause fracture deflection, and the fracturing pressure will rise rapidly (Fig. 2).

Drilling horizontal wellbores along the maximum horizontal principal stress direction, and the lowest fracturing pressure will be achieved during the fracturing operation. This will enable the fracture to initiate and expand directly at the perforation points, with the perforation points directly communicating with the artificial fractures. The artificial fractures created by the fracturing operation can also maximize communication with natural fractures, as most reservoir natural fractures typically develop perpendicular to the maximum horizontal principal stress direction. Additionally, based on the analysis of the experimental results of the angle between the maximum horizontal principal stress and the line of perforation hole arrangement and the fracturing pressure, both tubular wells and open-hole wells show that the fracturing pressure increases as the angle between the perforation hole and the maximum horizontal principal stress increases. Moreover, the rate of increase in the open-hole well is greater than that of the tubular well.

② Hole spacing

Hole spacing, defined as the number of perforations per unit depth of the wellbore, was set with a perforation azimuth of zero degrees and the perforation direction aligned with the maximum horizontal principal stress direction. According to existing experimental results, both hole spacing and the method of perforation significantly impact fracturing pressure. Specifically, spiral perforation typically exhibits a higher fracturing pressure than linear perforation by 6–8 MPa[44]. With the same perforation method, fracturing pressure decreases as hole spacing increases (Fig. 3).

As illustrated in Fig. 3, the relationship between fracturing pressure and perforation density is not a simple linear one. The fracturing pressure decreases as the perforation density increases from 2 to 8 holes per meter and from 8 to 16 holes per meter, but remains almost unchanged beyond 16 holes per meter. Notably, the fracturing pressure shows minimal change as the perforation density increases from 4 to 8 holes per meter and from 13 to 16 holes per meter.

This phenomenon can be attributed to the non-uniform interaction of multi-hole stress concentration effects as hole spacing decreases. Consequently, a perforation density of 16 holes per meter can be considered optimal, ensuring low fracturing pressure while mitigating potential issues related to excessive perforation on casing strength.

③ Perforation hole diameter

The diameter of the perforation hole is also a critical parameter in perforation design, influencing factors such as projectile selection. With a perforation density set at 16 holes per meter, research results shown in Fig. 4 indicate that the diameter of the perforation hole has a minimal effect on fracturing pressure.

④ Perforation hole length

Considering the impact of perforation hole length on fracturing pressure, a perforation density of 16 holes per meter was maintained. Calculations indicate that as the length of the perforation increases, the fracturing pressure exhibits a linear decline; however, this effect is relatively minor (Fig. 5).

Prediction of fracturing pressure after reservoir damage

The influence of reservoir damage on fracturing pressure is primarily evident in two aspects: Firstly, the skin effect induced by near-wellbore damage impacts the percolation capacity of fracturing fluid into the formation, leading to alterations in the circumferential stress at the wellbore and consequently affecting fracturing pressure. Secondly, following reservoir damage, changes in the mechanical properties of the rock further influence fracturing pressure.

Analysis of the impact of reservoir damage on formation stress

The changes in circumferential stress around the wellbore and the mechanical properties of rocks caused by skin effect due to reservoir damage near the wellbore can be attributed to the following factors.

a. *Drilling fluid invasion*: During drilling, the invasion of drilling fluid into the surrounding reservoir alters the mechanical properties of the reservoir rock. Solid particles and filtrate from the drilling fluid can clog pore spaces, reducing permeability and modifying key mechanical parameters such as elastic modulus and Poisson's ratio.

b. *Pressure differential effects*: The pressure difference between the inside and outside of the wellbore during drilling can alter the stress state of the reservoir rock. Significant pressure differentials subject the rock near the wellbore to increased stress, potentially leading to reduced rock strength and even shear or tensile failure.

c. *Chemical reactions induced by fluid invasion*: Chemical substances in the drilling fluid can react with the reservoir rock, altering its mineral composition and thereby affecting its mechanical properties. For example,
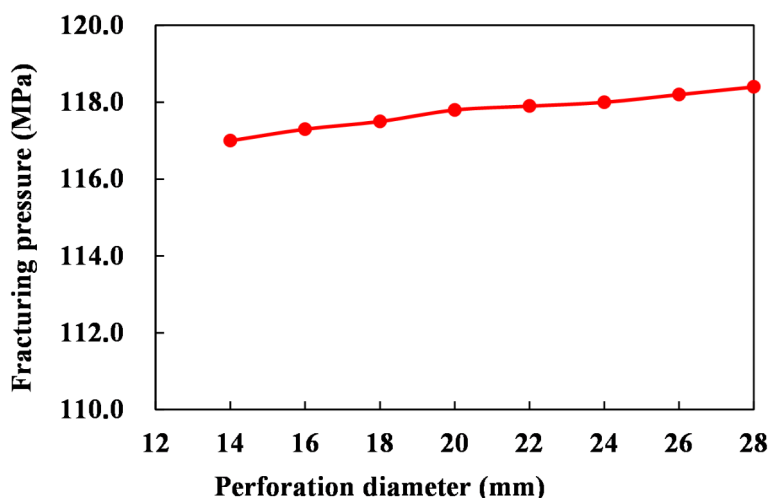

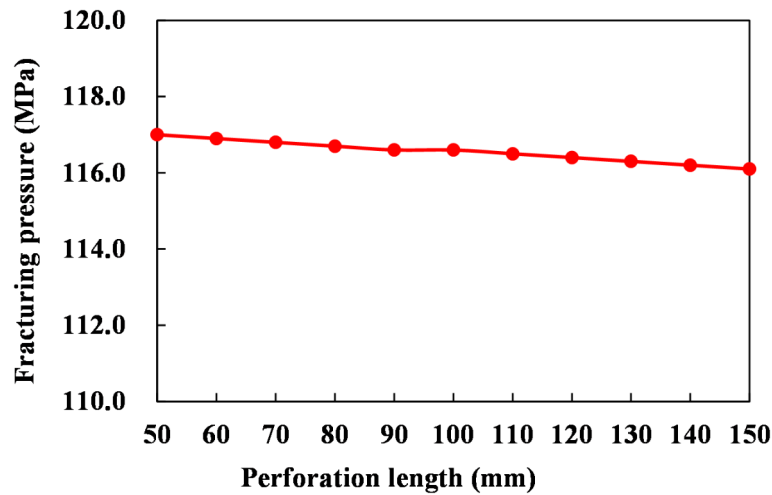**Fig. 4**. Relationship between the perforation diameter of well 1 and its fracturing pressure.

Fig. 5. Relationship between the perforation length of well 1 and its fracturing pressure.

certain components in the drilling fluid may interact with clay minerals, causing clay swelling and a reduction in rock strength.

d. *Temperature and pressure variations*: The high-temperature and high-pressure environment near the wellbore can influence both the physical and chemical properties of the reservoir rocks. Elevated temperatures may induce phase transitions in certain minerals, while high pressures can cause plastic deformation, further impacting the mechanical properties of the rock.

e. *Formation water intrusion*: During drilling, formation water may invade the reservoirs surrounding the wellbore, altering the pore structure and fluid properties of the reservoir. This intrusion can change the wettability of the reservoir rocks, thereby influencing their mechanical properties.

Stress field of open-hole completed wellbore post fracturing fluid invasion-induced damage

The presence of reservoir damage leads to an additional pressure drop as the fracturing fluid filters through the damage zone, which results in a decrease in the effective pumping pressure exerted on the formation. This reduction subsequently influences the additional stress generated by the radial infiltration of fracturing fluid into the formation. Furthermore, pore pressure also undergoes changes; thus, initial pore pressure cannot be regarded as a substitute. Consequently, conventional formulas for calculating stress induced by fracturing fluid filtration often yield certain inaccuracies due to overlooking the impact of damage.

Under the combined effect of wellbore pressure, geostress, and fracturing fluid seepage, a stress field distribution model around an open hole inclined wellbore was established based on the superposition principle using Eq. (19)

$$
\sigma_r = \frac{\sigma_H + \sigma_h}{2}\left(1 - \frac{r_i^2}{r^2}\right) + \left(\frac{\sigma_H - \sigma_h}{2}\right)\left(1 - 4\frac{r_i^2}{r^2} + 3\frac{r_i^4}{r^4}\right)\cos 2\theta + \frac{r_i^2}{r^2}P_i
$$
$$
+ \delta\left[\frac{\alpha(1-2\mu')}{2(1-\mu')}\left(1 - \frac{r_i^2}{r^2}\right) - \phi'\right](P_i - p(r,t))
\tag{19}
$$

$$
\sigma_\theta = \frac{\sigma_H + \sigma_h}{2}\left(1 + \frac{r_i^2}{r^2}\right) + \left(\frac{\sigma_H - \sigma_h}{2}\right)\left(1 + 3\frac{r_i^4}{r^4}\right)\cos 2\theta - \frac{r_i^2}{r^2}P_i
$$
$$
+ \delta\left[\frac{\alpha(1-2\mu')}{2(1-\mu')}\left(1 + \frac{r_i^2}{r^2}\right) - \phi'\right](P_i - p(r,t))
\tag{20}
$$

$$
\sigma_z = \sigma_z - 2\mu'(\sigma_H - \sigma_h)\frac{r_i^2}{r^2}cos2\theta + \delta\left[\frac{\alpha(1-2\mu')}{1-\mu'} - \varphi'\right](P_i - p(r,t))
\tag{21}
$$

$$
\tau_{r\theta} = \frac{\sigma_H + \sigma_h}{2}\left(1 - 3\frac{r_i^4}{r^4} + 2\frac{r_i^2}{r^2}\right)sin2\theta
\tag{22}
$$

When $r = r_w$, the stress component on the wellbore can be expressed as

$$
\sigma_r = P_i + \delta\varphi'(P_i - p(r,t))
\tag{23}
$$

$$
\sigma_\theta = -P_i + \delta\left[\frac{\alpha(1-2\mu')}{(1-\mu')} - \varphi'\right](P_i - p(r,t)) + \sigma_H(1 - 2cos2\theta) + \sigma_h(1 + 2cos2\theta)
\tag{24}
$$

$$\sigma_z = c\frac{r_i^2}{r^2}P_i + \sigma_v + \delta\left[\frac{\alpha\left(1-2\mu'\right)}{1-\mu'} - \varphi'\right]\left(P_i - p\left(r,t\right)\right) - 2\mu'\left(\sigma_H - \sigma_h\right)cos2\theta \quad (25)$$

where, $p\,(r,\,t)$—Pore pressure after fracturing fluid injection, MPa. p_i—Inject fracturing fluid pressure, MPa. ϕ'—Porosity of mud damage zone, %. μ'—Poisson's ratio of mud damage zone. δ—The permeability coefficient is $=\delta1$ when the formation is permeable and $=\delta0$ when the formation is impermeable. The original permeability, porosity, elastic modulus, and Poisson's ratio of the reservoir are porosity (ϕ), permeability (k), Elastic modulus (E) and Poisson's ratio (μ) respectively. The permeability, porosity, elastic modulus, and Poisson's ratio of the damage zone within the reservoir are ϕ', k', E', and μ', respectively. Then, the additional stress field caused by the radial infiltration of fracturing fluid into the surrounding rock layers around the wellbore after reservoir damage becomes that.

The above equation represents the final stress field of the wellbore after reservoir damage in an open hole deep well.

Stress field of near wellbore in perforated wells after reservoir damage

Using a stress solution method similar to that for open-hole wellbores and considering the presence of a well-consolidated cement sheath and formation, the fracturing fluid does not influence seepage from the wellbore into the formation. The stress on the perforation wall is calculated as follows:

$$\begin{cases} \sigma'_{pr} = \dfrac{r_{perf}^2}{L_{perf}^2}P_i + \delta\varphi'\left(p_i - p\left(r,t\right)\right) \\[2mm] \sigma'_{p\theta} = \left\{\begin{array}{l} -P_i + \sigma_H\left(1-2cos2\theta\right) + \sigma_h\left(1+2cos2\theta\right) \\ +c\dfrac{r_i^2}{r^2}P_i + \sigma_v - 2\mu'\left(\sigma_H - \sigma_h\right)cos2\theta \end{array}\right\} \\[6mm] \qquad -2\left\{\begin{array}{l} -P_i + \sigma_H\left(1-2cos2\theta\right) + \sigma_h\left(1+2cos2\theta\right)_p \\ -c\dfrac{r_i^2}{r^2}P_i - \sigma_v + 2\mu'\left(\sigma_H - \sigma_h\right)cos2\theta \end{array}\right\}cos2\theta' \\[6mm] \qquad -P_i + \delta\left[\dfrac{2\alpha\left(1-2\mu'\right)}{1-\mu'} - \varphi'\right]\left(p_i - p\left(r,t\right)\right) \\[4mm] \sigma'_{pz} = -2v'\left\{\begin{array}{l} -P_i + \sigma_H\left(1-2cos2\theta\right) + \sigma_h\left(1+2cos2\theta\right)_p \\ -c\dfrac{r_i^2}{r^2}P_i - \sigma_v + 2\mu'\left(\sigma_H - \sigma_h\right)cos2\theta \end{array}\right\}cos2\theta' \\[6mm] \qquad + P_i + \delta\varphi\left(p_i - p\left(r,t\right)\right) - cp_w \\[2mm] \qquad + \delta\left[\dfrac{\alpha\left(1-2\mu'\right)}{1-\mu'} - \varphi'\right]\left(p_i - p\left(r,t\right)\right) \end{cases} \quad (26)$$

After establishing a distribution model of the stress field around the wellbore of perforated well which formation was damaged by drilling fluid, the in-situ stress around the wellbore can be directly substituted into the formula for calculating the fracturing pressure for analysis.

Application results and analysis
Rock mechanics and geostress parameters for test wells

Rock mechanics parameter tests were conducted to obtain the rock mechanics parameters for two wells, as detailed in Tables 1, 2, 4, and 5. By substituting the parameter values from Tables 1 and 2 into Eq. (19), the fracture pressure for the open-hole completion of Well 1 was calculated and summarized in Table 3. Similarly, by substituting the parameter values from Tables 4 and 5 into Eq. (26), the fracture pressure for the perforated completion of Well 2 was determined and presented in Table 6.

Utilizing the computed layered stress values, static rock mechanics parameters, and additional test data, the breakdown pressure corresponding to each layer position under varying conditions can be accurately determined. The basic parameters of reservoir permeability and porosity, along with rock mechanics data, were input into the model to compute the fracture pressures for the two deep wells (Well 1 and Well 2) under different completion approaches.

The average rock mechanics parameters				
Depth of the well section (m)	6610.0–6622.0	6640.0–6650.0	6652.0–6664.0	6670.0–6674.0
Modulus of elasticity E (MPa)	44,431.4	40,670.3	46,794.8	35,406.8
Poisson's ratio	0.278	0.286	0.283	0.291

Table 1. The average rock mechanics parameters of Well 1 oil reservoir.

Depth of the well section (m)	Reservoir thickness (m)	Formation pressure (MPa)	Modulus of elasticity (MPa)	Poisson's ratio	Average density of overlying rock strata (kg/m³)
6610.0–6622.0	12.0	68.13	44,431.7	0.276	2500
6640.0–6650.0	10.0	68.38	40,670.2	0.288	2500
6652.0–6664.0	12.0	69.67	46,793.4	0.282	2500
6670.0–6674.0	4.0	70.13	35,406.8	0.290	2500

Table 2. Basic parameters of Well 1 oil reservoir section.

Depth of the well section (m)	6281.0–6287.0	6310.0–6331.0	6333.0–6335.0	6351.0–6357.0	6361.0–6370.0
Modulus of elasticity E (MPa)	40,241.0	46,464.3	36,622.8	49,942.7	48,527.2
Poisson's ratio	0.286	0.281	0.280	0.283	0.281

Table 4. The average rock mechanics parameters of Well 2 oil reservoirs.

Depth of the well section (m)	Reservoir thickness (m)	Formation pressure (MPa)	Modulus of elasticity (MPa)	Poisson's ratio	Average density of overlying rock strata (kg/m³)
6281.0–6287.0	6.0	65.47	40,241.0	0.286	2500
6310.0–6331.0	21.0	66.58	46,464.0	0.281	2500
6333.0–6335.0	2.0	66.38	39,622.8	0.283	2500
6351.0–6357.0	6.0	6657	49,942.7	0.283	2500
6361.0–6370.0	9.0	66.73	48,527.2	0.281	2500

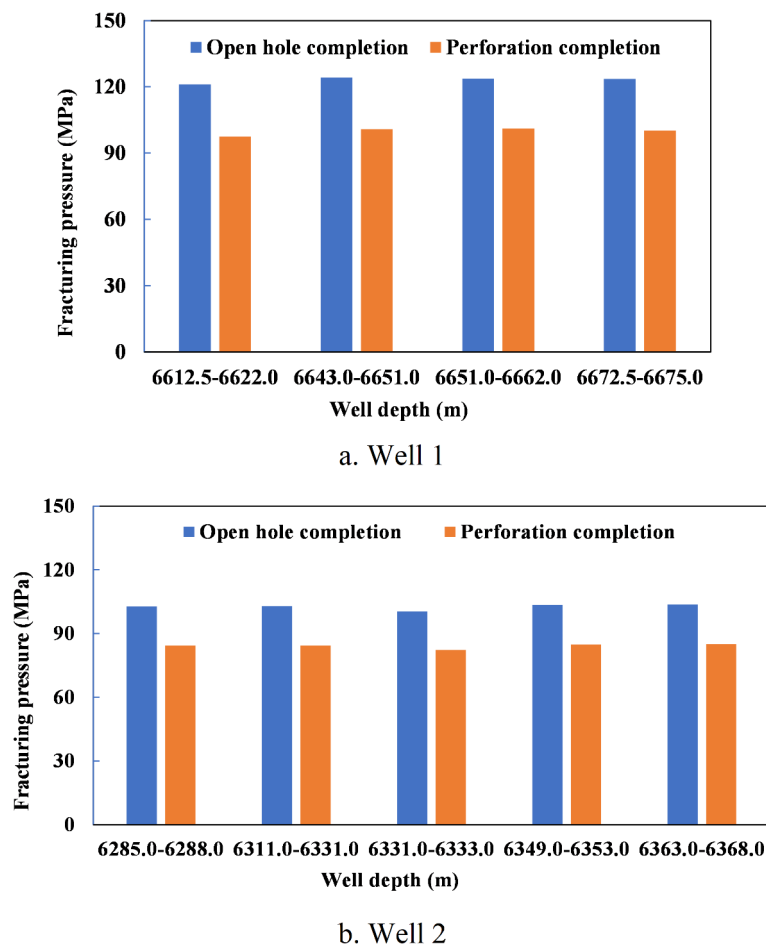**Table 5**. Basic parameters of Well 2 oil reservoir section.

Depth of the well section (m)	Minimum horizontal principal stress (MPa)	Maximum horizontal principal stresss (MPa)	Vertical principal stress (MPa)
6610.0–6622.0	103.1	121.7	151.7
6640.0–6650.0	104.2	120.9	151.9
6652.0–6664.0	106.1	125.2	153.1
6670.0–6674.0	104.2	118.3	153.6

Table 3. The calculated results of the geostress in the oil layer section of Well 1.

Depth of the well section (m)	Minimum horizontal principal stress (MPa)	Maximum horizontal principal stress (MPa)	Vertical principal stress (MPa)
6281.0–6287.0	96.73	111.71	137.8
6310.0–6331.0	98.31	115.93	139.27
6333.0–6335.0	96.51	111.39	138.98
6351.0–6357.0	99.63	118.47	138.73
6361.0–6370.0	99.54	117.79	139.93

Table 6. The calculated results of the geostress in the oil layer section of Well 2.

Results and analysis

A comprehensive comparative analysis of breakdown pressures and their gradients for reservoir rocks was conducted between perforated completions and open-hole completions, as illustrated in Figs. 6 and 7. This study aimed to evaluate the differences in fracturing pressure characteristics under different wellbore configurations, providing valuable insights into optimal completion strategies.

The results derived from the reservoir rock fracturing pressure prediction model reveal significant variations between the two completion methods. For Well 1, the fracturing pressure gradient for the open-hole completion ranges from approximately 0.0182–0.0190 MPa/m. In contrast, the perforated completion exhibits a lower gradient, ranging from approximately 0.0142–0.0152 MPa/m. This difference can be attributed to the distinct hydraulic conditions and stress distributions associated with each completion method. The open-hole

a. Well 1

b. Well 2

Fig. 6. Calculation results of rock fracturing pressure in Well 1 with different completion.

configuration allows for more direct interaction between the formation and the fracturing fluid, potentially leading to higher pressure gradients due to less resistance compared to the perforated completion, where the presence of casing and cement sheath may introduce additional constraints.
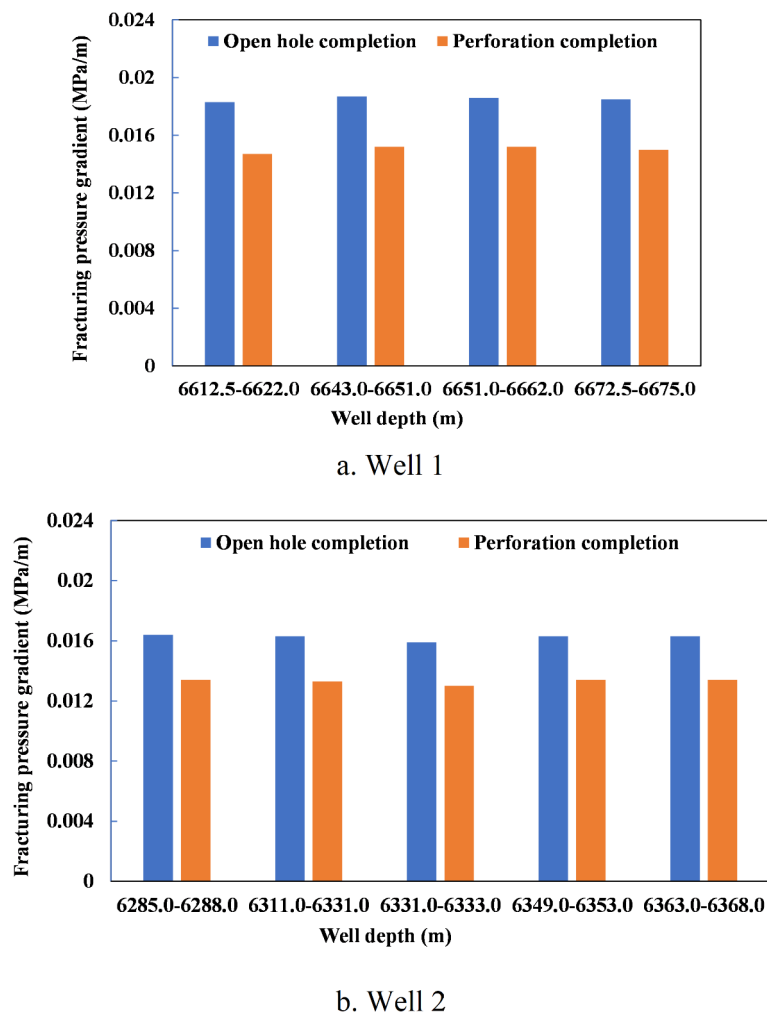
For Well 2, similar trends were observed. The fracturing pressure gradient for the open-hole completion ranges from approximately 0.0158–0.0165 MPa/m, while that for the perforated completion ranges from approximately 0.0130–0.0135 MPa/m. These findings highlight the importance of considering specific geological and engineering factors when selecting an appropriate completion method. The lower pressure gradients in perforated completions suggest that this method may be more suitable for formations with lower permeability or where minimizing injection pressure is a priority.

Furthermore, the analysis underscores the need for detailed modeling and site-specific data collection to accurately predict fracturing pressure gradients. Factors such as formation heterogeneity, in-situ stress conditions, and the mechanical properties of the rock play crucial roles in determining the effectiveness of each completion approach. By understanding these variations, engineers can make informed decisions to optimize fracturing operations, enhance production efficiency, and ensure well integrity.

A comparative analysis of perforated completions and open-hole completions reveals that perforated completions offer a significant advantage in reducing formation fracturing pressures. This benefit arises from the strategic placement of perforations at designated locations within the wellbore, which effectively alleviates portions of the in-situ stress, thereby diminishing the load on surrounding rock masses.

During perforation operations, specialized tools are employed to create precise holes through the casing and cement sheath into the formation. These perforations serve multiple purposes: they enhance flow channels for hydrocarbons within the reservoir and significantly mitigate instability phenomena associated with high pressure. By providing additional pathways for fluid flow, perforations help distribute pressure more evenly across the formation, thus reducing localized stress concentrations that could lead to fractures or other forms of instability.

Research indicates that following the implementation of perforation technology, a more uniform stress distribution emerges among various layers of the reservoir. This uniformity is crucial for preventing local instabilities and maintaining reservoir integrity. The even distribution of stress helps avoid excessive deformation or failure in specific areas, ensuring overall structural stability during production activities.

a. Well 1

b. Well 2

Fig. 7. Calculation results of rock fracturing pressure gradient in Well 1 with different completion.
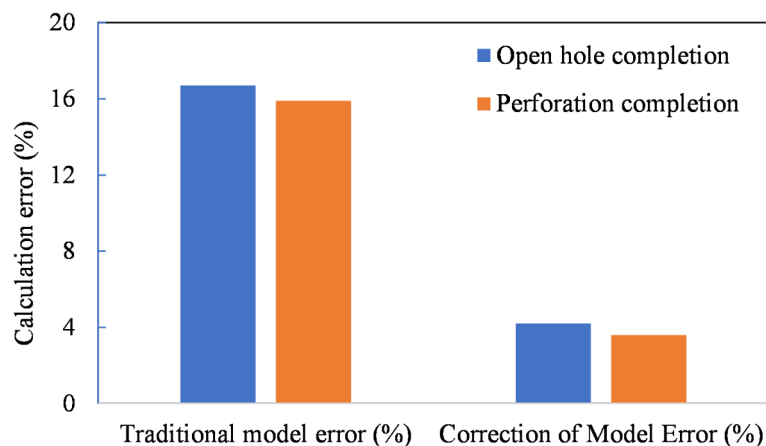
Based on these calculations, it is evident that perforated completions can reduce formation fracturing pressures by 10–15%. This reduction is particularly advantageous in formations characterized by exceptionally high fracturing pressures, where traditional open-hole completions may pose higher risks of inducing fractures or causing reservoir damage. By lowering the required fracturing pressure, perforated completions facilitate safer and more efficient extraction processes.

A unified fracture pressure model has been developed for both open-hole and perforated wells to enable direct mechanical comparison between the two completion methods. This model provides a quantitative basis for optimizing completion strategies. It reveals the mechanisms of stress redistribution following fracturing fluid invasion and reservoir damage, correcting errors in predicting fracture pressures in contaminated formations. According to the calculation and analysis of two wells, the error in predicting rupture pressure has been reduced by approximately 10% (Fig. 8).

Consequently, this technology finds extensive application in challenging geological settings such as deep and ultra-deep wells, tight formations, and reservoirs with complex stress regimes. In these environments, the ability to control and manage fracturing pressures is critical for optimizing production rates while minimizing potential risks. Perforated completions not only enhance operational safety but also extend the productive life of the well by preserving reservoir integrity over time. Comparative analysis highlights the advantages of perforated completions in reducing formation fracturing pressures. By strategically creating perforations, this method effectively manages in-situ stresses, improves fluid flow, and ensures a more uniform stress distribution throughout the reservoir. These benefits make perforated completions an indispensable tool for safe and efficient hydrocarbon extraction, particularly in formations characterized by high fracturing pressures.

Conclusions

(1) A fracturing pressure model was developed for various completion methods, specifically open-hole completions and cased perforated completions. The analysis demonstrates that cased perforated completions significantly reduce the reservoir's fracturing pressure, with a reduction range of 10–15%. Formation dam-

Fig. 8. Error analysis of fracture pressure value calculated by correcting the model.

age introduces pore-scale effects, alters rock mechanical parameters, and modifies the stress distribution around the wellbore in post-damage scenarios. These changes can substantially increase the reservoir's fracturing pressure.

(2) The stress concentration around the wellbore is a function of the angle between the maximum horizontal principal stress direction and the perforation orientation, while the fracturing pressure depends on this angular relationship. When the perforation holes are aligned parallel to the maximum horizontal principal stress direction, the fracturing pressure reaches its minimum value. Conversely, when they are oriented perpendicular to this direction, the fracturing pressure attains its maximum value. The optimal perforation orientation for effectively reducing formation fracturing pressure lies within $\pm 40°$ of the maximum horizontal principal stress direction. Exceeding this range may cause deviations in fracture propagation, leading to a rapid increase in fracturing pressure.

(3) Perforation density and configuration significantly influence the fracturing pressure in cased wells. For a given perforation configuration, fracturing pressure decreases progressively as perforation density increases; conversely, the diameter and length of perforation holes have relatively minor effects on the reservoir's fracturing pressure. Understanding these relationships is essential for optimizing completion strategies to enhance hydrocarbon recovery while minimizing risks associated with fracturing operations.

Data availability
The datasets used and/or analyzed during the current study available from the corresponding author on reasonable request.

References
1. Shiyi, Y. U. & Qiang, W. A. New progress and prospect of oilfields development technologies in China. *Pet. Explor. Dev.* **45**(4), 698–711 (2018).
2. Qun, L. E. et al. Technological progress and prospects of reservoir stimulation. *Petrol. Explor. Dev.* **46**(3), 605–613. https://doi.org/10.1016/S1876-3804(19)60040-6 (2019).
3. Li, Q. et al. Synthetic process on hydroxyl-containing polydimethylsiloxane as a thickener in CO_2 fracturing and thickening performance test. *Energy Sour. Part A: Recovery, Utiliz. Environ. Effects* **40**(9), 1137–1143 (2018).
4. Yan, X. et al. Fracture plugging zone for lost circulation control in fractured reservoirs: Multiscale structure and structure characterization methods. *Powder Technol.* **370**, 159–175 (2020).
5. Li, Q. et al. Wellhead stability during development process of hydrate reservoir in the northern south china sea: Evolution and mechanism. *Processes* **13**(1), 40 (2024).
6. Setiyawan, H., Widagdo, J. A., Dewi, C. K., Evelyn, K., Pambudi, T., Ramadhani, U., Prayoga, A., Afton, M., Joestiawan, A. P. A new breakthrough of horizontal well stimulation: Improving oil production through stimulation cleanup-Jetacid method in waterflood North area. In *IADC/SPE Asia pacific drilling technology conference and exhibition?* p. D021S012R006. (SPE, 2024).
7. Li, S. et al. Simulation and control strategies for longitudinal propagation of acid fracture in a low-permeability reservoir containing bottom water. *Processes* **12**, 792. https://doi.org/10.3390/pr12040792 (2024).
8. Xu, C. et al. Experimental study on fracture plugging effect of irregular-shaped lost circulation materials. *Energy.* **1**(276), 127544 (2023).
9. Chengyuan, Xu., Liu, L., Yang, Y., Kang, Y. & You, Z. An innovative fracture plugging evaluation method for drill-in fluid loss control and formation damage prevention in deep fractured tight reservoirs. *Fuel* **358**, 130123 (2024).
10. Yao, P. et al. Effect of water occurrence in coal reservoirs on the production capacity of coalbed methane by using NMR simulation technology and production capacity simulation. *Geoenergy Sci. Eng.* **243**, 213353. https://doi.org/10.1016/j.geoen.2024.213353 (2024).
11. Rutqvist, J. & Stephansson, O. The role of hydromechanical coupling in fractured rock engineering. *Hydrogeol. J.* **11**, 7–40 (2003).
12. Becerra, D. et al. Evaluation of reservoir quality and forecasted production variability along a multi-fractured horizontal well. Part 1: Reservoir characterization. *Energies* **14**(19), 6154 (2021).

13. Hyman, J. D. et al. Understanding hydraulic fracturing: A multi-scale problem. *Philos. Trans. Royal Soc. A: Math. Phys. Eng. Sci.* **374**(2078), 20150426 (2016).
14. Lecampion, B., Bunger, A. & Zhang, X. Numerical methods for hydraulic fracture propagation: A review of recent trends. *J. Natural Gas Sci. Eng.* **1**(49), 66–83 (2018).
15. Li, S. et al. True triaxial physics simulations and process tests of hydraulic fracturing in the Da'anzhai section of the Sichuan Basin tight oil reservoir. *Front. Energy Res.* **2**(11), 1267782 (2023).
16. Damjanac, B., Gil, I., Pierce, M., Sanchez, M., Van As, A. & McLennan, J. A new approach to hydraulic fracturing modeling in naturally fractured reservoirs. In *ARMA US rock mechanics/geomechanics symposium* pp. ARMA-10. (ARMA, 2010).
17. Ehlers, W. & Luo, C. A phase-field approach embedded in the theory of porous media for the description of dynamic hydraulic fracturing. *Comput. Methods Appl. Mech. Eng.* **1**(315), 348–368 (2017).
18. Kroon, M. & Faleskog, J. A probabilistic model for cleavage fracture with a length scale-influence of material parameters and constraint. *Int. J. Fract.* **118**, 99–118 (2002).
19. Fjaer, E., Holt, R. M., Horsrud, P., Raaen, A. M. & Risnes, R. Mechanics of hydraulic fracturing. *Dev. Petrol. Sci.* **1**(53), 369–390 (2008).
20. Ostadhassan M. Geomechanics and elastic anisotropy of shale formations. New Frontiers in Oil and Gas Exploration. 165–207 (2016).
21. Thomas, N. & Weijermars, R. Comprehensive atlas of stress trajectory patterns and stress magnitudes around cylindrical holes in rock bodies for geoscientific and geotechnical applications. *Earth-Sci. Rev.* **1**(179), 303–371 (2018).
22. Haimson, B. C. & Chang, C. True triaxial strength of the KTB amphibolite under borehole wall conditions and its use to estimate the maximum horizontal in situ stress. *J. Geophys. Res.: Solid Earth* **107**(B10), ETG-15 (2002).
23. Shahid, A. S. A., Fokker, P. A. & Rocca, V. A review of numerical simulation strategies for hydraulic fracturing, natural fracture reactivation and induced microseismicity prediction. *Open Petrol. Eng. J.* **9**(1), 72–91 (2016).
24. Powlay, B., Karakus, M., Amrouch, K. & Chester, C. Effects of notches on breakdown pressures and fracture evolution in hydraulic fracturing. *Rock Mech. Rock Eng.* **19**, 1–4 (2024).
25. Vallejo, L. E. Shear stresses and the hydraulic fracturing of earth dam soils. *Soils Found.* **33**(3), 14–27 (1993).
26. Genter, A., Evans, K., Cuenot, N., Fritsch, D. & Sanjuan, B. Contribution of the exploration of deep crystalline fractured reservoir of Soultz to the knowledge of enhanced geothermal systems (EGS). *Comptes Rendus Geosci.* **342**(7–8), 502–516 (2010).
27. Gilbert, J. R. Assessing the risks and benefits of hydraulic fracturing. *Mo. Envtl. L. Pol'y Rev.* **18**, 169 (2010).
28. Seco, E., Pinto, P. S. & Maranha Das Neves, E. (1985). Hydraulic fracturing in zoned earth and rockfill dams. In *International conference on soil mechanics and foundation engineering*. pp. 2025–2030 (1985).
29. Mori, A. & Tamura, M. Hydrofracturing pressure of cohesive soils. *Soils Found.* **27**(1), 14–22 (1987).
30. Cheng, Y., Yan, C. & Han, Z. Mechanics of hydraulic fracturing. In *Foundations of rock mechanics in oil and gas engineering* pp. 213–268. (Singapore: Springer Nature Singapore, 2023).
31. Bjerrum, L., Nash, J. K., Kennard, R. M. & Gibson, R. E. Hydraulic fracturing in field permeability testing. *Geotechnique* **22**(2), 319–332 (1972).
32. Li, S. et al. Simulation of filtration fields with different completion methods in carbonate gas reservoirs. *Chem. Technol. Fuels Oils* **57**, 698–704 (2021).
33. Nguyen, H. T., Lee, J. H. & Elraies, K. A. Review of pseudo-three-dimensional modeling approaches in hydraulic fracturing. *J. Petrol. Exp. Product. Technol.* **12**(4), 1095–1107 (2022).
34. Ismail, A. & Azadbakht, S. A comprehensive review of numerical simulation methods for hydraulic fracturing. *Int. J. Numer. Anal. Methods Geomech.* **48**(5), 1433–1459 (2024).
35. Detournay, E. & Cheng, A. H. D. Fundamentals of poroelasticity. In *Comprehensive rock engineering* Vol. 2, (1993).
36. Zimmerman, R. W. *Rock physics and geomechanics* (Elsevier, 1991).
37. Segall, P. *Earthquake and volcano deformation* (Princeton University Press, 2010).
38. Dengsheng, Y. *Theory and research of reducing reservoir abnormal burst pressure* 45–50 (SouthWest Petroleum University, 2008).
39. Kang, Y., Yu, M., Miska, S. & Takach, N. E. Wellbore stability: A critical review and introduction to DEM. In *SPE Annual Technical Conference and Exhibition?* pp. SPE-124669. (SPE, 2009).
40. Ibrahim, A. A review of mathematical modelling approaches to tackling wellbore instability in shale formations. *J. Nat. Gas Sci. Eng.* **89**, 103870 (2021).
41. Cai, W. M., Murti, V. & Valliappan, S. Slope stability analysis using fracture mechanics' approach. *Theor. Appl. Fract. Mech.* **12**(3), 261–281 (1990).
42. Zeng, F., Cheng, X., Guo, J., Chen, Z. & Xiang, J. Investigation of the initiation pressure and fracture geometry of fractured deviated wells. *J. Petrol. Sci. Eng.* **165**, 412–427 (2018).
43. Qu, Z. et al. Optimization on fracturing fluid flowback model after hydraulic fracturing in oil well. *J. Petrol. Sci. Eng.* **204**, 108703 (2021).
44. Wang, Q. et al. Numerical simulation of fracture initiation, propagation and fracture complexity in the presence of multiple perforations. *J. Nat. Gas Sci. Eng.* **83**, 103486 (2020).

Author contributions

Yanlin Zhang: Conceptualization, writing—original draft. Yang Tian: project administration, resources, writing—original draft. Lina Sun Project administration, resources, investigation, methodology. Zhufeiye Yuan and Yi Wang: visualization, conceptualization. All authors have read and agreed to the published version of the manuscript.

Declarations

Competing interests

The authors declare no competing interests.

Additional information

Correspondence and requests for materials should be addressed to Y.T. or Z.Y.

Reprints and permissions information is available at www.nature.com/reprints.

Publisher's note Springer Nature remains neutral with regard to jurisdictional claims in published maps and institutional affiliations.